ADVANCED MATERIALS
www.advmat.de

www.MaterialsViews.com

Sequential Infiltration Synthesis of Doped Polymer Films with Tunable Electrical Properties for Efficient Triboelectric Nanogenerator Development

*Yanhao Yu, Zhaodong Li, Yunming Wang, Shaoqin Gong, and Xudong Wang**

Triboelectric nanogenerator (TENG) is rising as a promising technology for converting mechanical energy into electricity with merits of high output, simple design, and low cost.[1,2] Recent research efforts have largely improved its power density and thus enabled a number of applications varying from driving small electronics, to charging batteries, and to activating chemical reactions.[3–12] The working principle of TENG is based on the combined effect triboelectrification and electrostatic induction. Specifically, upon the contact of two dissimilar surfaces (mostly polymer) with different electron affinities, electrons transfer across the interface to compensate for the difference of surface potentials. This charge separation is the primary principle of mechanical to electric energy conversion.[1,13] A typical TENG design possesses two electrodes attached to the triboelectrific active materials, where electrostatic charges are induced. Once the device capacitance changes (e.g., by displacement), current flow occurs between the two conductive electrodes and thus outputs electric power. Therefore, controlling the charge density on the triboelectric surfaces is the most fundament strategy for improving the performance of TENG. Nowadays, surface modification of triboelectric polymer is the predominate approach to regulate the charge density. For instance, morphologies like nanowire,[14–19] nanoparticle,[20] or other nanoscale patterns[21,22] are frequently adopted to raise the surface area of triboelectric materials and thus enable more charge carrying site. In addition, surface functionalization[13] and ionized species[23] can also be introduced to improve the charge density on polymer surfaces. However, operation of TENGs requires intimate contact and sometimes friction between the triboelectric materials, which inevitably induces wearing of surface. In this regard, surface modification/engineering yields little contributions toward the performance gain in long-term operation. Therefore, one essential solution is to extend the property engineering from mere surface to the bulk of material.

Y. Yu, Z. Li, Prof. X. D. Wang
Department of Material Sciences and Engineering
University of Wisconsin-Madison
Madison, WI 53706, USA
E-mail: xudong@engr.wisc.edu
Dr. Y. Wang, Prof. S. Gong
Department of Biomedical Engineering
and Wisconsin Institutes for Discovery
University of Wisconsin-Madison
Madison, WI 53706, USA

DOI: 10.1002/adma.201502546

Atomic layer deposition (ALD) is a powerful thin film growth technique on the basis of sequential self-limiting surface reactions.[24,25] When implemented to certain polymer materials, the large permittivity of metalorganic precursors allows deep infiltration of the inorganic compounds during the ALD process, leading to inorganic/organic hybrid materials.[26–32] This process is known as sequential infiltration synthesis (SIS).[33,34] It has been successfully used to convert the block co-polymer nanopatterns into more durable inorganic patterns[35–37] and to improve the polymeric lithography resistance to subsequent etching.[38–40] Inspired by this development, we expect SIS could effectively tailor the internal composition and electrical properties of polymer films, which may provide an ultimate solution for triboelectric material design in the development of high-performance TENGs. In this Communication, we report an internal AlO_x doping of several polymers via SIS, including polydimethylsiloxane (PDMS), polyimide (Kapton), and poly(methyl methacrylate) (PMMA). We showed that SIS can introduce AlO_x molecules ≈3 µm deep into these polymers, which effectively tuned the bulk electrical property of the film. TENG devices using the modified polymer films exhibited enhanced power output; and this enhancement remained effective after the surface of polymer film was polished off for more than 2 µm. This polymer doping approach opens a new route to bulk electrical property modification of polymer films, demonstrating a promising strategy for improving the performance of functional polymer based devices, such as TENGs.

AlO_x was selected as the inorganic material to dope the polymer film since trimenthy aluminum (TMA, ALD precursor of Al_2O_3) has desirable permittivity in a number of polymers including polystyrene, polypropylene, polyethylene, poly(vinyl chloride), and PMMA.[32] A homemade ALD system was applied to sequentially introduce TMA and H_2O vapor toward the polymer film at 80 °C with controlled exposure time and cycles. The SIS doping process followed a typical ALD operation procedure except that the supplying time of TMA was extended to 5 s to promote its infiltration into the polymer film (see the Experimental Section for details). The infiltration results were first characterized by scanning electron microscopy (SEM) and energy dispersive spectroscopy (EDS). **Figure 1**a,b shows the cross-sectional images and corresponding elemental mappings of the pristine PDMS film and the same film after 5-cycle sequential TMA/H_2O infiltration (marked as AlO_x-doped PDMS), respectively. PDMS elements including silicon (Si), oxygen (O), and carbon (C) were all identified uniformly distributed in the pristine film and no aluminum (Al) signal was detected (Figure 1a, ii–v). From

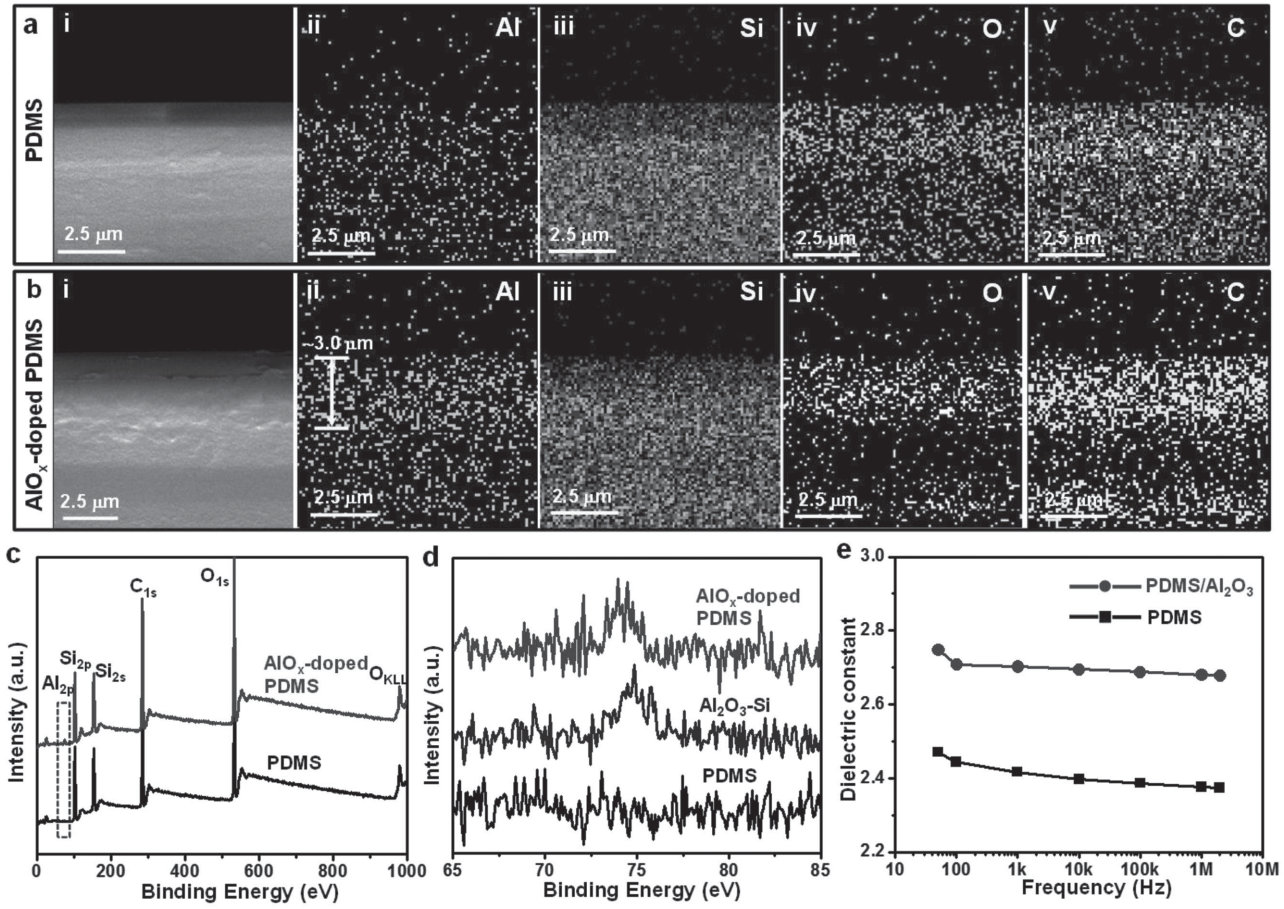

Figure 1. Elemental characterizations of AlO_x-doped PDMS film. a,b) Cross-sectional SEM images (i) and EDS mappings of a) a pristine PDMS film and b) an AlO_x-doped PDMS film for Al, Si, O, and C elements (ii–v). c) Full range XPS spectrum acquired from an AlO_x-doped PDMS film, where small Al 2p peak was detected. d) Al 2p scan for pristine PDMS, AlO_x-doped PDMS film, and ALD grown Al_2O_3 on silicon substrate. The peak position shift indicates the presence of defective oxides in AlO_x-doped PDMS film. e) Dielectric constant measured from pristine PDMS and AlO_x-doped PDMS, showing enlarged dielectric constant of PDMS due to the AlO_x doping.

the SIS-treated PDMS film, Al signal was clearly detected and was concentrated within the top ≈3 μm region revealing the effective infiltration depth (Figure 1b, ii). No Al signal could be detected deeper inside the film (Figure S1, Supporting Information). Other than the Si element that was still uniformly distributed in the entire PDMS film (Figure 1b, iii), both O and C elements exhibited a concentrated signal within the top ≈3 μm region that was in good accordance with Al distribution. The concentrated O element could be attributed to H_2O precursor infiltration that reacted with TMA forming Al—O bonds. The unreacted methyl groups on TMA could be the main source responsible for the concentrated C signal. This elemental distribution analysis evidences the successful deep infiltration of both precursors in the polymer film and no surface coating of Al_2O_3 was identified.

The elemental feature and bonding state of AlO_x-doped PDMS film were further studied by X-ray photoelectron spectroscopy (XPS). Figure 1c shows the XPS spectra of both pristine PDMS and AlO_x-doped PDMS samples. The characteristic peaks of PDMS including Si 2p, Si 2s, C 1s, O 1s, and O KLL peaks were identified from both films. From the AlO_x-doped PDMS sample, a small signal of Al 2p also appeared in the low binding energy region, suggesting the existence of Al element. To reveal the chemical environment of Al inside the polymer, Al 2p spectrum was individually scanned and compared with Al 2p peak of standard ALD-grown Al_2O_3 on silicon substrate (Figure 1d). The shift of peak position from 75.6 to 74.7 eV evidenced the presence of unstable defective oxides such as Al_2O and AlO.[41] The nonstoichiometric aluminum oxide may introduce extra charge carrier sites, which could raise the total charge capacitance of AlO_x-doped PDMS film and therefore enhance the output of TENGs. To evaluate this hypothesis, the dielectric constant was measured from both PDMS films. As shown in Figure 1e, AlO_x doping raised the dielectric constant from ≈2.4 of the pristine PDMS to ≈2.7 within the testing frequency range. Higher dielectric constant suggests that the AlO_x-doped PDMS film could handle more induced electrostatic charges resulted from the triboelectric effect.

The deep infiltration of Al is attributed to the good solubility of TMA precursor in the polymer material. With the similar chemical property, diethylzinc (DEZ) also exhibited excellent infiltration capability into PDMS to dope PDMS with ZnO_x. EDS elemental mapping of the PDMS film after 5-cycle SIS of DEZ and H_2O clearly identified Zn elements within the top

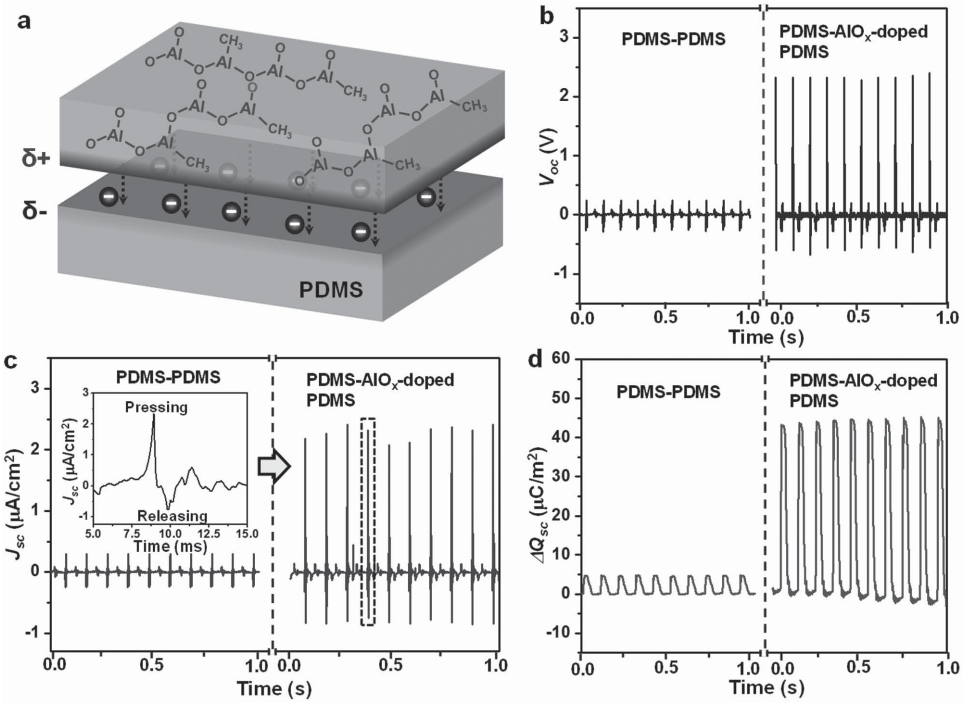

Figure 2. Design and performance of AlO_x-doped PDMS TENG. a) Schematic of charge redistribution between pristine PDMS and AlO_x-doped PDMS films upon contact as a consequence of triboelectrification. b) The open-circuit voltage (V_{oc}), c) short-circuit current density (J_{sc}), and d) charge transfer amount under short-circuit condition (ΔQ_{sc}) of TENGs composed of PDMS with and without AlO_x doping. The inset in (c) is the enlarged current output (dashed square box in (c)) created by one pressing and releasing cycle.

of ≈4 μm region (Figures S2 and S3, Supporting Information). Because inorganic precursors typically exhibit very limited solubility in organic polymer materials, they are not desirable for SIS polymer doping. As a demonstration, titanium tetrachloride ($TiCl_4$) and vanadium oxytrichloride ($VOCl_3$) were applied to infiltrate PDMS. EDS elemental mapping of the PDMS film after 5-cycle SIS of $TiCl_4$ and $VOCl_3$ revealed nearly none Ti and V signal from the entire cross-section region (Figures S4 and S5, Supporting Information). However, it should be noted that TiO_x, VO_x, and other metal oxides doping in polymers are expected to be effective if metal organic ALD precursors like titanium isopropoxide (TTIP) and vanadium oxytriisopropoxide (VTIP) were used.[42] The broad selection of metal organic ALD precursors evidences the excellent flexibility of the SIS technique in triboelectric polymer doping.

Typically, materials with distinct electron affinities (i.e., maximum difference in the tendency to gain or repulse electrons from each other) are desired to maximize the charge generation upon contact for high-performance TENG design.[13] Same materials or materials with close electron affinities are not able to produce appreciable electric output. The SIS doping technique allows us to arbitrarily tune the bulk electron affinities of polymer materials and thus largely broadens the material choices. To elucidate this advantage, the SIS doping enhancement in triboelectrific charge generation was investigated using a simple double-layered configuration (the TENG design is schematically shown in Figure S6, Supporting Information) and compared with the untreated materials. The testing devices were built with an identical size (1 cm × 1 cm × 260 μm) on flexible indium tin oxide/polyethylene terephthalate (ITO/PET) substrates (see the experimental details in the Experimental Section). Since AlO_x and PDMS have strong tendency in repulsing and gaining electron, respectively,[1,43,44] the AlO_x doping is expected to significantly lower electron affinity of intrinsic PDMS. This could enable considerable charge redistribution between the pristine PDMS and AlO_x-doped PDMS friction surfaces (**Figure 2**a). Upon the contact of PDMS and AlO_x-doped PDMS films, electrons were injected from the AlO_x-doped PDMS to PDMS film as a consequence of the large difference of electron affinity. Subsequently, positive (σ^+) and negative (σ^-) charges accumulated on the AlO_x-doped PDMS and PDMS films, respectively, offering the primary electric energy stored between the two electrodes. Upon the separation of the two surfaces, the stored electric energy was released in the form of current flow through the external circuit, which was recorded as current and voltage pulses. On the other hand, if two identical PDMS films without any modification or functionalization were brought together, they would not create the redistribution of surface charge and would result in negligible electric outputs. Figure 2b–d compares typical open-circuit voltage (V_{oc}), short-circuit current density (J_{sc}), and the total amount of charge transferred under short-circuit condition (ΔQ_{sc}) of TENGs with these two configurations. For the device composed of AlO_x-doped PDMS, the average peak values of the V_{oc}, J_{sc}, and ΔQ_{sc} reached 2.3 V, 2.2 μA cm^{-2}, and 45 μC m^{-2}, respectively. The J_{sc} and ΔQ_{sc} values are comparable with the performance of TENGs made from two typical triboelectric materials with distinct electron affinities such as PDMS-ITO[22] and teflon-metal[23] pairs. Whereas, only 0.3 V of V_{oc}, 0.3 μA cm^{-2} of J_{sc}, and 5 μC m^{-2} of ΔQ_{sc} were detected

for the untreated PDMS pair. Although theoretically, the PDMS pair was not supposed to exhibit any electric output, the small signal might be caused by the slight variation of PDMS films in terms of size, thickness, and surface roughness. The electrical property engineered by SIS doping was found very durable. A TENG device was repeatedly tested for 60 days and no deterioration of output voltage could be identified (Figure S7, Supporting Information).

An individual peak profile of the *J*–*t* curve further reveals the influence of AlO_x doping to the electron affinity of PDMS films. During the measurement, the positive and negative electrodes of the current meter were connected to pristine PDMS and AlO_x-doped PDMS films, respectively. Therefore, positive signal represents current flow from the pristine PDMS to AlO_x-doped PDMS, and vice versa. As shown in the inset of Figure 2c, a positive current pulse was generated first when both surfaces were brought into contact, suggesting electrons were moved from AlO_x-doped PDMS electrode to pristine PDMS electrode. This evidenced the AlO_x doping enabled strong tendency of giving away electrons to the untreated PDMS. When the two surfaces were detached, the local charge equilibrium was broken again and electrons flew back generating a negative current pulse. The AlO_x-doped PDMS and pristine PDMS films were also assembled with traditional positive (PMMA) and negative (polytetrafluoroethylene, PTFE) triboelectric materials. Due to the reduced electron affinity, enhanced output was obtained from the pair of PTFE-AlO_x-doped PDMS, while PMMA-AlO_x-doped PDMS exhibited reduced output (Figure S8, Supporting Information). These results further evidenced this SIS polymer doping strategy can be effectively and generally applied to polymer-based TENG devices.

To further investigate the SIS doping effect, multiple PDMS films were subjected to SIS doping with different cycles and then assembled into TENG devices with identical configuration as described previously (Figure S6, Supporting Information). The open circuit voltage was tested under identical conditions as the measure of their electrical property variation. The peak V_{oc} was plotted as a function of the SIS cycle and shown in **Figure 3**a. It was found that only two cycles of SIS were able to boost the average value of V_{oc} from 0.3 to 1.9 V, suggesting the high effectiveness of this polymer modification approach. The V_{oc} further increased following the SIS cycles and saturated at ≈2.4 V after ten cycles of infiltration. The V_{oc} variation is believed to be closely related to the unique reaction process of SIS AlO_x in polymer materials. During the first approximately ten cycles of infiltration synthesis, TMA diffused into PDMS and accumulated inside the polymer film, resulting in the rapid increase of V_{oc}. Further deposition might saturate the surface layer and prevent further infiltration inside. Thus the growth mode switched back to regular ALD deposition of continuous Al_2O_3 film on the surface.[24] Because additional cycles of infiltration contributed no internal doping, the electric property and corresponding triboelectric voltage output would not exhibit any further change. This investigation reveals the up limit of the SIS doping strategy.

Compared to conventional surface modification/functionalization, a unique merit of SIS doping is the property engineering in bulk volume, which is substantially important for TENG application because of the inevitable wearing issue during operation. To illustrate this merit, we polished the AlO_x-doped PDMS film to different level and measured the performance of corresponding TENG devices. As shown in Figure 3b, the polymer film was still capable of delivering ≈95% of the highest V_{oc} after the top ≈2 µm was polished away from the polymer surface. This favorable outcome can be intuitively expected since the detectable penetration depth of AlO_x was ≈3 µm and considerable amount of AlO_x still existed in the PDMS film with a tailored electric property after the removal of top ≈2 µm. After removing ≈3 µm PDMS from the surface, the voltage output started to reduce dramatically and eventually reached the minimal V_{oc} at ≈0.3 V when more than ≈5 µm polymer was removed. The minimal voltage output was at the same level as that generated by a pair of untreated PDMS surfaces (Figure 2b) because of the complete removal of AlO_x dopants in the polymer. The insets of Figure 3b compare the

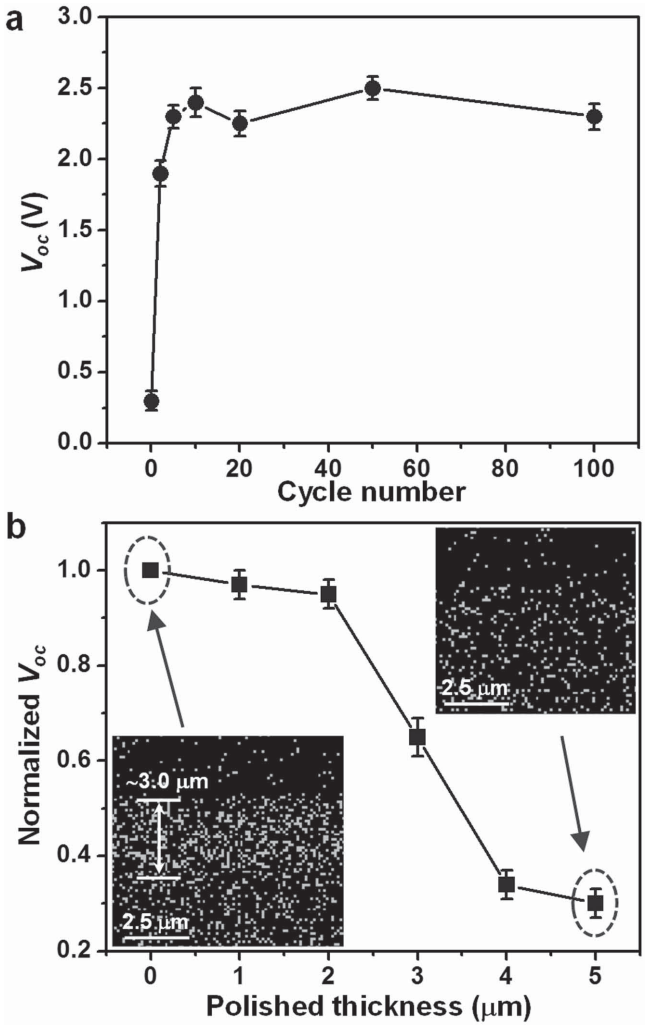

Figure 3. Doping cycle and performance evaluation of AlO_x-doped PDMS TENG. a) V_{oc} variation versus the doping cycles of AlO_x on PDMS film. b) Normalized V_{oc} of TENGs as a function of the material thickness that was polished off. Voltage output of AlO_x-doped PDMS film without any polishing was defined as unit. Insets are Al element EDS mapping of AlO_x-doped PDMS films before (left) and after (right) ⩾5 µm polishing.

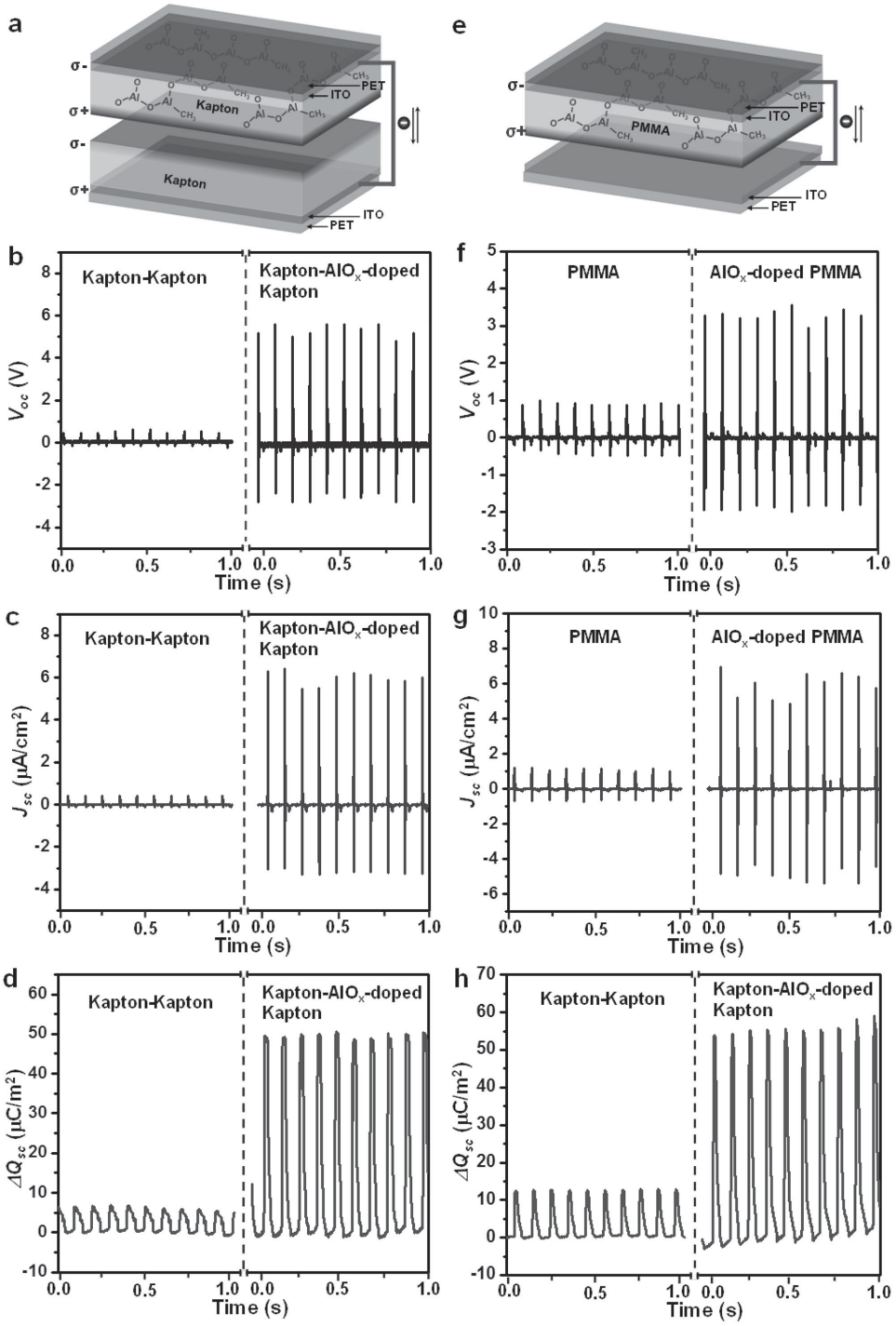

Figure 4. Design and performance of a–d) AlO_x-doped Kapton and e-h) AlO_x-doped PMMA TENGs. a) Schematically illustration of AlO_x-doped Kapton TENGs with a configuration of pristine Kapton/ITO/PET as the bottom electrode and AlO_x-doped Kapton/ITO/PET as the top electrode. b) V_{oc}, c) J_{sc}, and d) ΔQ_{sc} of TENGs made from Kapton with and without AlO_x doping. e) Schematic of AlO_x-doped PMMA TENGs with a configuration of ITO/PET as the bottom electrode and AlO_x-doped PMMA/ITO/PET as the top electrode. f) V_{oc}, g) J_{sc}, and h) ΔQ_{sc} characterizations of TENGs assembled from PMMA with and without AlO_x doping.

EDS mappings of PDMS film before and after removing the top ≈5 μm material, confirming the absence of Al element.

This SIS doping strategy is versatile in engineering the property of a broad range of polymer materials because of the appreciable permittivity of the metalorganic precursor within most polymer chains.[24] As a demonstration, two more polymers, Kapton and PMMA, were selected for SIS AlO_x doping. EDS analysis confirmed successful infiltration of Al-containing

molecules. For both materials, the depth of infiltration is ≈3 um for five cycles of SIS, which is similar to PDMS (Figures S9 and S10, Supporting Information). Based on the polymer's intrinsic electron affinity, the output of voltage could be tuned toward different directions. Similar to PDMS, Kapton has strong capability of acquiring electrons and always presents a negatively charged surface when contacts most other materials. By SIS doping of AlO_x, the electron affinity of Kapton could be significantly reduced, same as PDMS. When AlO_x-doped Kapton was brought together with a pristine Kapton film for triboelectrific charge generation, drastic electron transfer was enabled from AlO_x-doped Kapton to untreated Kapton leaving positive charges on the AlO_x-doped Kapton surface and the other one charged negatively (**Figure 4**a). Based on the same operating mechanism described for the PDMS case, triboelectrific outputs were substantially increased by SIS doping. As shown in Figure 4b–d, the AlO_x-doped Kapton TENG device yielded average peak values of 5.1 V for V_{oc}, 5.6 μA cm^{-2} for J_{sc}, and 47 μC m^{-2} for ΔQ_{sc}, which were approximately one order of magnitude higher than those generated by the untreated Kapton pairs.

Different from PDMS and Kapton, PMMA is a polymer with a strong tendency to give away electrons when contacts other materials. This is the same capability offered by AlO_x doping. Therefore, higher positive charge density can be expected by introducing AlO_x doping into PMMA. Such enhancement is highly desirable for raising the performance of TENGs built with dissimilar materials since it increases the top limit of induced free charges that in turn raises the maximum triboelectrific output. To demonstrate this effect, a TENG device was assembled using AlO_x-doped PMMA and ITO as two contacting surfaces (schematically shown in Figure 4e). In this design, electrons are always injected from PMMA to ITO surface during the contact and results in the accumulation of positive electrostatic charge on the PMMA surface. Figure 4f–h compares the triboelectrific outputs of PMMA-based TENGs with and without AlO_x doping. The measurements clearly showed that upon AlO_x doping, the V_{oc} was improved from 0.9 to 3.1 V, J_{sc} was raised from 1.0 μA cm^{-2} to 5.5 μA cm^{-2}, and ΔQ_{sc} was increased from 12 μC m^{-2} to 54 μC m^{-2}. Such a significant enhancement is the consequence of increased positive charge density on the PMMA surface due to AlO_x infiltration.

In summary, the SIS technique was successfully applied to infiltrate AlO_x molecules into polymer films and tune their electrical properties. TMA precursor was found to be able to travel into various polymer materials (e.g., PDMS, Kapton, and PMMA) with a diffusion depth of ≈3 μm under mild deposition conditions and form AlO_x species inside the polymer film. Due to the AlO_x molecules' strong tendency of repulsing electron, the electron attaining capability of AlO_x-doped polymer with strong electron affinity was significantly reduced compared to its original state. This effect allows the creation of high-performance TENG devices with the same polymer materials. If the host polymer has the same trend of repulsing electron as the AlO_x dopant, such as PMMA, the capacitance of induced charge can be raised and significant performance gain of TENG devices can be expected. Furthermore, different from surface modification/functionalization that was commonly implemented in TENG performance tuning, the SIS doping changes the polymer's bulk property. Therefore, the resulted enhancement would not be diminished even after the polymer surface was worn during long-term operation. Therefore, the SIS doping strategy holds a great promise in tuning the performance of polymer-based electronic or dielectric devices, such as TENGs for effective mechanical energy harvesting.

Experimental Section

Fabrication of Polymer Films: PDMS films were made from a mixture of liquid PDMS elastomer and cross-linker with a ratio of 10:1, which was uniformly casted on a flat silicon substrate. After degasing in vacuum for 20 min and curing at 80 °C for 2 h, a PDMS film was received. PMMA films were fabricated by spin-coating the liquid precursor onto ITO/PET substrate at 2000 rpm for 120 s and annealing at 70 °C for 30 min. The liquid precursor was made by dissolving PMMA powder (molecular weight: ≈550 000) into chlorobenzene solvent with a concentration of 4 wt%. Commercial Kapton and PTFE tape was directly attached to ITO/PET substrate for TENG assembly. For the wearing test of AlO_x-doped PDMS, the polymer film was polished using the tripod method[45] with a speed of 30 rpm. The finest sandpaper (100 nm) was used to achieve maximal flatness of the polished surface.

Doping Polymer via SIS: A home-made ALD system was used to infiltrate AlO_x into the polymer films. The target polymer film was loaded on a quartz boat and placed at the position 5 cm away from the precursor inlet nozzle. N_2 gas with a flow rate of 40 sccm was introduced into the chamber as the carrier gas, which yielded a base pressure of 650 mTorr. The chamber temperature was maintained at 80 °C during the entire infiltration process. TMA and H_2O vapors were pulsed into the deposition chamber separately with a pulsing time of 5 and 1 s, respectively, and separated by 60 s N_2 purging. Therefore, one SIS cycle involves 1 s of H_2O pulse + 60 s of N_2 purging + 5 s of TMA pulse + 60 s of N_2 purging. After the infiltration, the chamber was cooled down naturally under N_2 flow. The DEZ, $TiCl_4$, and $VOCl_3$ infiltration experiments were conducted following the same procedure of AlO_x penetration except replacing TMA with DEZ, $TiCl_4$, and $VOCl_3$.

Assembly and Measurements of TENGs: For PDMS- and Kapton-based TENGs, AlO_x-doped polymer films with a size of 1 cm × 1 cm were attached to the center of an ITO/PET substrate (2 cm × 5 cm), which was considered as the top electrode. Bottom electrode was composed of an unmodified polymer film with the same size and location on another ITO/PET substrate. Two electrodes were separated by two pieces of glass spacers (1 mm in thickness) and connected to the external circuit through copper tapes. For PMMA-based TENGs, a blank ITO/PET and an ITO/PET attached with a AlO_x-doped PMMA film (1 cm × 1 cm) were used as the bottom and top electrodes, respectively. For PDMS/PTFE and PDMS/PMMA TENGs, PDMS with or without AlO_x doping (1 cm × 1 cm) was attached on ITO/PET substrate as the top electrode. PTFE and PMMA film (1 cm × 1 cm) attached on ITO/PET substrate were used as the bottom electrode. During the performance measurement, the top electrode was pressed to the bottom electrode by a computer-controlled shaker with a frequency of 10 Hz and the bottom electrode was anchored on the table surface. The voltage outputs were recorded using an Agilent DSO1012A oscilloscope. The current outputs and charge transfer amount of TENGs were measured using an Autolab PGSTAT302N station.

Morphology and Elemental Characterizations: SEM measurements and EDS mappings were performed on Zeiss Leo 1530 field-emission microscope. XPS was conducted on a Thermo Scientific K-alpha XPS instrument. The survey range was from 0 to 1000 eV. The Al 2p spectra were measured for characterizing the chemical structures of AlO_x in the

PDMS film. Dielectric constant measurements were conducted on the Agilent E4980A Precision LCR Meter.

Supporting Information

Supporting Information is available from the Wiley Online Library or from the author.

Acknowledgements

The authors thank Professor Paul Voyles and Ms. Pei Zhang for helping with the polishing process and access to the tripod polishing machine. This work was primarily supported by the U.S. Department of Energy (DOE), Office of Science, Basic Energy Sciences (BES), under Award No. DE-SC0008711.

Received: May 28, 2015
Revised: June 17, 2015
Published online: July 15, 2015

[1] Z. L. Wang, *ACS Nano* **2013**, *7*, 9533.
[2] S. Wang, L. Lin, Z. L. Wang, *Nano Energy* **2015**, *11*, 436.
[3] S. Wang, L. Lin, Z. L. Wang, *Nano Lett.* **2012**, *12*, 6339.
[4] Y. Yang, H. Zhang, Z.-H. Lin, Y. Liu, J. Chen, Z. Lin, Y. S. Zhou, C. P. Wong, Z. L. Wang, *Energy Environ. Sci.* **2013**, *6*, 2429.
[5] X. S. Zhang, M. D. Han, R. X. Wang, F. Y. Zhu, Z. H. Li, W. Wang, H. X. Zhang, *Nano Lett.* **2013**, *13*, 1168.
[6] S. Kim, M. K. Gupta, K. Y. Lee, A. Sohn, T. Y. Kim, K. S. Shin, D. Kim, S. K. Kim, K. H. Lee, H. J. Shin, D. W. Kim, S. W. Kim, *Adv. Mater.* **2014**, *26*, 3918.
[7] K. Y. Lee, J. Chun, J. H. Lee, K. N. Kim, N. R. Kang, J. Y. Kim, M. H. Kim, K. S. Shin, M. K. Gupta, J. M. Baik, S. W. Kim, *Adv. Mater.* **2014**, *26*, 5037.
[8] Q. Zheng, B. Shi, F. Fan, X. Wang, L. Yan, W. Yuan, S. Wang, H. Liu, Z. Li, Z. L. Wang, *Adv. Mater.* **2014**, *26*, 5851.
[9] G. Zhu, W. Q. Yang, T. Zhang, Q. Jing, J. Chen, Y. S. Zhou, P. Bai, Z. L. Wang, *Nano Lett.* **2014**, *14*, 3208.
[10] Y. Mao, D. Geng, E. Liang, X. Wang, *Nano Energy* **2015**, *15*, 227.
[11] W. Seung, M. K. Gupta, K. Y. Lee, K. S. Shin, J. H. Lee, T. Y. Kim, S. Kim, J. Lin, J. H. Kim, S. W. Kim, *ACS Nano* **2015**, *9*, 3501.
[12] W. Tang, Y. Han, C. B. Han, C. Z. Gao, X. Cao, Z. L. Wang, *Adv. Mater.* **2015**, *27*, 272.
[13] S. H. Shin, Y. H. Kwon, Y. H. Kim, J. Y. Jung, M. H. Lee, J. Nah, *ACS Nano* **2015**, *9*, 4621.
[14] L. Zheng, Z.-H. Lin, G. Cheng, W. Wu, X. Wen, S. Lee, Z. L. Wang, *Nano Energy* **2014**, *9*, 291.
[15] Y. Li, G. Cheng, Z.-H. Lin, J. Yang, L. Lin, Z. L. Wang, *Nano Energy* **2015**, *11*, 323.
[16] L. Lin, Y. Xie, S. Niu, S. Wang, P. K. Yang, Z. L. Wang, *ACS Nano* **2015**, *9*, 922.
[17] M. Kanik, M. G. Say, B. Daglar, A. F. Yavuz, M. H. Dolas, M. M. El-Ashry, M. Bayindir, *Adv. Mater.* **2015**, *27*, 2367.
[18] P. Bai, G. Zhu, Q. Jing, J. Yang, J. Chen, Y. Su, J. Ma, G. Zhang, Z. L. Wang, *Adv. Funct. Mater.* **2014**, *24*, 5807.
[19] Y. Su, X. Wen, G. Zhu, J. Yang, J. Chen, P. Bai, Z. Wu, Y. Jiang, Z. Lin Wang, *Nano Energy* **2014**, *9*, 186.
[20] G. Zhu, Z. H. Lin, Q. Jing, P. Bai, C. Pan, Y. Yang, Y. Zhou, Z. L. Wang, *Nano Lett.* **2013**, *13*, 847.
[21] C. K. Jeong, K. M. Baek, S. Niu, T. W. Nam, Y. H. Hur, D. Y. Park, G. T. Hwang, M. Byun, Z. L. Wang, Y. S. Jung, K. J. Lee, *Nano Lett.* **2014**, *14*, 7031.
[22] F. R. Fan, L. Lin, G. Zhu, W. Wu, R. Zhang, Z. L. Wang, *Nano Lett.* **2012**, *12*, 3109.
[23] S. Wang, Y. Xie, S. Niu, L. Lin, C. Liu, Y. S. Zhou, Z. L. Wang, *Adv. Mater.* **2014**, *26*, 6720.
[24] S. M. George, *Chem. Rev.* **2010**, *110*, 111.
[25] M. Leskelä, M. Ritala, *Thin Solid Films* **2002**, *409*, 138.
[26] B. Gong, J. C. Spagnola, S. A. Arvidson, S. A. Khan, G. N. Parsons, *Polymer* **2012**, *53*, 4631.
[27] B. Gong, H. Kim do, G. N. Parsons, *Langmuir* **2012**, *28*, 11906.
[28] R. Saberi Moghaddam, S. Huettner, Y. Vaynzof, C. Ducati, G. Divitini, R. H. Lohwasser, K. P. Musselman, A. Sepe, M. R. Scherer, M. Thelakkat, U. Steiner, R. H. Friend, *Nano Lett.* **2013**, *13*, 4499.
[29] R. P. Padbury, J. S. Jur, *J. Vac. Sci. Technol. A* **2014**, *32*, 041602.
[30] Q. Peng, Y. C. Tseng, S. B. Darling, J. W. Elam, *Adv. Mater.* **2010**, *22*, 5129.
[31] J. D. Ferguson, A. W. Weimer, S. M. George, *Chem. Mater.* **2004**, *16*, 5602.
[32] C. A. Wilson, R. K. Grubbs, S. M. George, *Chem. Mater.* **2005**, *17*, 5625.
[33] M. Biswas, J. A. Libera, S. B. Darling, J. W. Elam, *J. Phys. Chem. C* **2015**, *119*, 14585.
[34] Q. Peng, Y. C. Tseng, S. B. Darling, J. W. Elam, *ACS Nano* **2011**, *5*, 4600.
[35] J. Meyer, P. Görrn, F. Bertram, S. Hamwi, T. Winkler, H.-H. Johannes, T. Weimann, P. Hinze, T. Riedl, W. Kowalsky, *Adv. Mater.* **2009**, *21*, 1845.
[36] J. Yin, Q. Xu, Z. Wang, X. Yao, Y. Wang, *J. Mater. Chem. C* **2013**, *1*, 1029.
[37] J. Kamcev, D. S. Germack, D. Nykypanchuk, R. B. Grubbs, C. Y. Nam, C. T. Black, *ACS Nano* **2013**, *7*, 339.
[38] Y.-C. Tseng, Q. Peng, L. E. Ocola, D. A. Czaplewski, J. W. Elam, S. B. Darling, *J. Vac. Sci. Technol. B: Microelectron. Nanometer Struct.* **2011**, *29*, 06FG01.
[39] Y.-C. Tseng, Q. Peng, L. E. Ocola, J. W. Elam, S. B. Darling, *J. Phys. Chem. C* **2011**, *115*, 17725.
[40] Y.-C. Tseng, Q. Peng, L. E. Ocola, D. A. Czaplewski, J. W. Elam, S. B. Darling, *J. Mater. Chem.* **2011**, *21*, 11722.
[41] H.-S. Kang, M. Siva Pratap Reddy, D.-S. Kim, K.-W. Kim, J.-B. Ha, Y. S. Lee, H.-C. Choi, J.-H. Lee, *J. Phys. D: Appl. Phys.* **2013**, *46*, 155101.
[42] A. Sinha, D. W. Hess, C. L. Henderson, *J. Vac. Sci. Technol. B* **2007**, *25*, 1721.
[43] C. Y. Guo, A. T. Hong Tang, J. K. Hon Tsoi, J. P. Matinlinna, *J. Mech. Behav. Biomed. Mater.* **2014**, *32*, 145.
[44] A. F. Diaz, R. M. Felix-Navarro, *J. Electrost.* **2004**, *62*, 277.
[45] P. M. Voyles, J. L. Grazul, D. A. Muller, *Ultramicroscopy* **2003**, *96*, 251.